IEEE Access
Multidisciplinary | Rapid Review | Open Access Journal

Received June 18, 2019, accepted July 9, 2019, date of publication July 15, 2019, date of current version August 1, 2019.

*Digital Object Identifier 10.1109/ACCESS.2019.2928629*

# A 3D-Printed High-Dielectric Filled Elliptical Double-Ridged Horn Antenna for Biomedical Monitoring Applications

**SIAMAK SARJOGHIAN, (Graduate Student Member, IEEE), MD HASANUZZAMAN SAGOR, (Member, IEEE), YASIR ALFADHL, (Senior Member, IEEE), AND XIAODONG CHEN, (Fellow, IEEE)**

School of Electronic Engineering and Computer Science, Queen Mary University of London, London E1 4NS, U.K.

Corresponding author: Siamak Sarjoghian (s.sarjoghian@qmul.ac.uk)

**ABSTRACT** A novel wideband (WB) 3D-printed elliptical double-ridged horn (EDRH) antenna filled with a high-dielectric material (i.e., a mixture of the paraffin and titanium oxide ($TiO_2$)) is proposed for medical monitoring systems. The antenna has been designed and optimized to operate in the frequency range (2–6 GHz) to satisfy an optimal penetration level and to maintain a WB operation, which results in a high-resolution detection. The proposed antenna is embedded into a high-dielectric material to miniaturize its size and to further reduce the reflections due to mismatch with the body. The antenna was tested on tissue models consisting of two layers (i.e., skin and muscle). The reflection coefficients of the antenna, when it is on the modeled tissue, have been generated and compared with the reference of –6 dB. The obtained results show that the antenna benefits from the 4 GHz of bandwidth with a gain of 5–8 dB within the operating region.

**INDEX TERMS** 3D printing, antenna, double-ridged horn, high-dielectric material, WB.

## I. INTRODUCTION

The WIDEBAND (WB) technique is a promising wireless technology, which uses radio waves for transferring data over a very high bandwidth; i.e., typically equal or more than 500 MHz. This technique is termed based on the ultra-wideband (UWB) technology that originally aimed for short-range wireless communication channels [1].

The wideband operation requires a low power level and is ideal for short-range communications, and can be useful for medical sensing applications. It utilizes a large portion of the radio spectrum that can improve the speed and reduce interference of data transfer compared with other technologies in the market.

The independent regulator and competition authority for the UK Communications Industries (Ofcom) and the Federal Communications Commission (FCC) regulation of the UWB in the US, have defined the regulation for the UWB technology that allows the unlicensed operating within range of 3.1 GHz to 10.6 GHz, and 41.3 dBm/MHz transmitted power [2]. Stating the UWB technique principles, it is limited to the specific frequency band by the authorities, which may smear a limitation in the biomedical application that aims to scan inside the human body, due to the demand of lower frequency and therefore better penetration depth [3]. However, the evidence states that the UWB provides an acceptable penetration depth for biomedical applications related to scanning the upper layers of the body surface such as the skin, muscle, and fat [4]–[6].

Therefore, the WB technique was proposed to overcome using any center frequency. In this technique, the signals diffuse across a wide range of frequencies to detect thicknesses of layered samples accurately.

The technique advantages from a wider bandwidth in comparison with the other technologies that enable this method to send trains of pulses containing hundreds of millions of pulses per second. The systems operating in this band tend to have small dimension and consume very low power, hence, they fit the requirement for use as an indoor application. In the last few years, the WB technique has been selected as

The associate editor coordinating the review of this manuscript and approving it for publication was Abhishek Kandwal.

a good candidate for medical and scanning applications, due to its properties, e.g. low power, high data rates, multipath immunity, simultaneous ranging and communication [1].

The elliptical double-ridged horn (EDRH) antenna was first introduced in 1950 [7], although the concept of the ridged-waveguides was introduced earlier in 1947 [8]. This antenna has attracted engineers and researchers in the radar field, based on its advantages such as large bandwidth, and high gain/directivity [9]–[11].

These important principles make this type of antenna an efficient solution for biomedical applications that aims to scan inside humans' body, as compared with the other bidirectional types, e.g. bowtie, and three-dimensional folded antenna [12]. Besides the advantages, the antenna suffers from higher fabrication cost due to the shape complexity, and also the large aperture for low-frequency applications (2–6 GHz).

Operating at this frequency range is vital for selecting an appropriate penetration depth on the human body. Therefore, a center frequency of 3.1 GHz was chosen to analyses this system behavior, as this frequency is optimal for these medical applications. In order to overcome the cost of fabrication, different types of 3D printing techniques have been proposed by engineers, which use different materials such as metal and an acrylonitrile butadiene styrene (ABS) [13], [14].

Three-dimensional (3D) printing using metal materials is a costly solution. The surface of the fabricated design using the material is noticeably rough that can reduce the band [15], [16]. Hence, in-house 3D printing using the ABS technique is selected as an optimal alternative solution, concerning the cost and the ease of fabrication. To overcome the complications of 3D printing method, a diverse set of solutions have been provided as such, a low-conductive surface due to having a rough surface, as well as the inaccessible painting areas that are resolved by printing the antenna in two sections from the middle and to further glue them together after inside being printed. Other concerns of the design have been the bulky structure of the EDRH antenna at a low frequency, and the large reflections, which needs to be minimized by matching the medium with the antenna. Earlier studies have addressed this, by embedding the antenna inside high dielectric material, e.g., ceramics, oil, and pure water [17]–[19].

The cost and fabrication method of designs using high-dielectric ceramic, have made researchers think of other solutions, e.g. pure water that has a low-conductivity due to the elimination of particles in water. Moreover, after an extended work conducted on the distilled or deionized types of water to be loaded in the antenna as a high dielectric.

The highest amount of energy transmitted from the existing source will be absorbed within the antenna structure. This energy absorption is due to the molecule structure and the high conductivity of the water even after particles elimination. Alternative oil material has been defined as the optimal liquid solution due to its low-conductivity, although suffering from a low-permittivity as well as not having a fixed shape when it is loaded in the antenna.

The contributions of this work can be summarized as follows:

1) The proposed elliptical double-ridged horn antenna has a shape that not only comforts the finalized system, but also improved the operation, e.g. directivity, gain, and bandwidth to some extent compared to the similar designs.

2) The high dielectric material with the low conductivity used to miniaturize the design and reduce the reflection within the system. Moreover, the material has advantages, e.g. easy and low cost to manufacture into the required shape.

3) The extension was proposed and added to the antenna in order to eliminate the signal-overlapping issue in the case of using the antenna as a transceiver in a system as well as propagating plane wave into the medium.

The rest of this paper is organized as follows.

Section II presents the characterization of the dielectric properties for the desired frequency region. Section III presents, the antenna design and evaluation using the simulated results that used the data retrieved in the previous section. Section IV presents, the antenna fabrication and measurements using the in-house equipment; e.g., the 3D-printer and vector network analyzer (VNA). Section V provides the discussion, followed by Section VI that concludes the paper.

## II. MATERIALS CHARACTERIZATION

Different dielectric liquids and their mixtures with high-permittivity and low-conductivity materials have led to the conclusion that a particular type of oil, e.g. canola oil, is of interest due to its low-conductivity, low-cost, and safety for skin-based biomedical monitoring systems [20]. However, using a liquid for a biomedical system is not optimal, and hence, the better solution of solid material, such as paraffin was used.

The open-ended coaxial probe method was established as one of the principal methods for the dielectric measurement of various materials [21]. This method has been selected and applied to characterize and validate the materials. The PNA-L network analyzer, dielectric probe, and electronic calibration (ECal) module have been used to measure the dielectric properties. The instrument was calibrated with the distilled water, presented in Fig. 2, to increase the accuracy of the results at the room temperature (i.e. 20°C) for all the experimental results using the VNA, ECal kit and open-ended probe setup, as in Fig. 1. The off-the-shelf paraffin container wax was selected with a density of around $0.83-0.86$ g/cm$^3$ at 15°C and a melting point of 45°C [22]. This paraffin was chosen as a preliminary dielectric material, due to its solubility, flexibility and lower conductivity compared to the other materials. The measured dielectric properties of the paraffin, as shown in Figs. 3 (a) and (b), indicate the low-conductivity and permittivity at the frequency of 3.1 GHz ($\varepsilon_r \sim 2.16$ and $\sigma \sim 0.003$). Hereby, as an attempt

**FIGURE 1.** The in-house measurement setup based on the open-ended coaxial probe technique, used for the characterization of the dielectric materials.

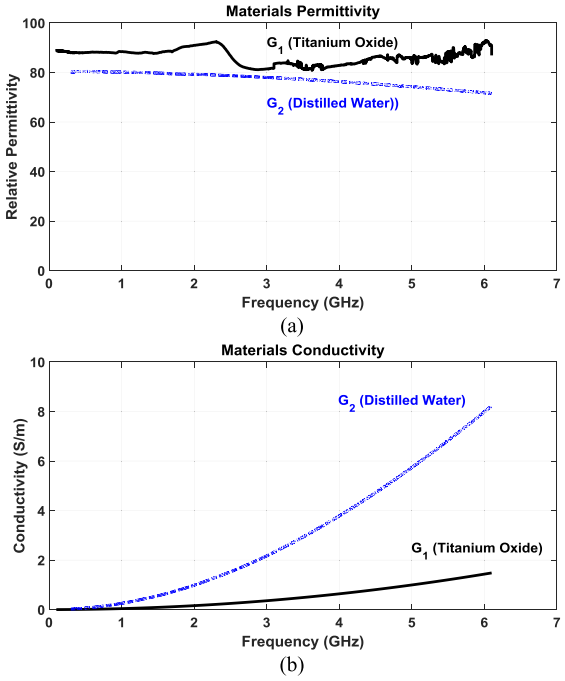


**FIGURE 2.** (a) measured permittivity; (b) conductivity of r-$TiO_2$ in black line and water in blue dashed line at 0.3–6.1 GHz.

to introduce a novel method to increase the permittivity of the deployed paraffin, it has been further mixed with the titanium dioxide ($TiO_2$) to increase the permittivity of the material [23]. This process has been repeated with different mix percentages. An optimal mixture has been chosen for the materials that provides a decent homogeneity. In this regard, the conductivity of the mixture has increased with reference to the $TiO_2$ conductivity, but the conductivity is still in the acceptable range, not to disturb the wave propagation. The frequency of 3.1 GHz is chosen for the proposed system, based on the tissue penetration capability, and the required bandwidth.

Based on trace metal analysis the rutile-$TiO_2$ (r-$TiO_2$) powder with an average particle size of $\leq$100 nm and a purity of 99.5% (by Sigma Aldrich) was chosen. The selection r-TiO2 in this work was due to its prime factors such higher permittivity and melting points, as well as lower conductivity compared to other types (e.g. anatase and brookite) [24], [25].

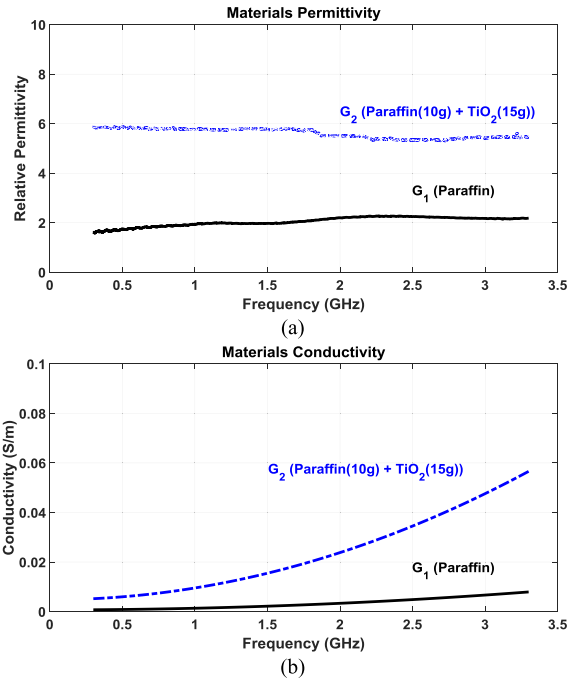


**FIGURE 3.** (a) measured permittivity; (b) conductivity of paraffin in black line and its mixture with r-$TiO_2$ in blue dashed line at 0.3–3.3 GHz.

The powder is currently employed in different products, such as sun protection creams, paints and high-dielectric ceramic due to its high refractive index capability and high dielectric constant. The powder is sintered using the spark plasma sintering (SPS) method at the temperature of 1250°C [26].

The dielectric properties of the sintered r-$TiO_2$ sample are measured using the open-ended probe method shown in Fig. 2. It was noticed that results at higher frequencies suffer certain irregular fluctuation. This could be attributed to the unavoidable diminishingly small air-gap that developed during the experiment between the sample and probe. The small air-gap error is minimal at a lower frequency as it is expected.

The proposed r-$TiO_2$ white powder has been mixed with the paraffin at the temperature around 70°C (i.e., well above the melting point), to increase the permittivity of the material. This ceramic powder benefits from the increased permittivity; it is non-invasive to the skin and can be applied by oil to eliminate the air gap when the antenna is placed on the body. To increase the permittivity and ensure the low-conductivity of the material required for the design, different portions of each material are mixed and the dielectric properties are measured. The ideal two portions of the paraffin (40g) were heated to 70°C to form into the liquid and three portions of the r-$TiO_2$ (60g) were gradually mixed with the paraffin to the saturation point. The mixture was shaken well to remove the bubbles and left to cool down and turning to solid form.

Furthermore, to check the homogeneity of the mixture, the material properties are measured across a number of locations of a premade large sample. The absolute measurements

(rather than the average values) are also compared and the results have further exhibited a very good consistency, which in turn can be translated into an acceptable assumption that the effective permittivity is homogeneous.

The measured dielectric properties of the sample in the frequency range of 0.3–3.3 GHz was obtained and shown in Fig. 3. The measured permittivity of the mixture is more than twice as the paraffin with a slightly higher conductivity at the frequency of 3.1 GHz ($\varepsilon_r \sim 5.4$ and $\sigma \sim 0.004$).

This mixture is proposed for any high dielectric embedded antenna design, which can be used in the biomedical imaging systems. There are a number of advantages in using such a high dielectric material in a radar-oriented system, which operates on the human body as such, reducing the size of the antenna and the reflections due to the mismatch and forming a flexible case of embedding material for a specific structure.

## III. ANTENNA DESIGN AND EVALUATION

The horn antenna has been considered as one of the universal microwave antennas in technical deployment for many years. Moreover, among different types of horn antennas, the EDRH has attracted researchers in the medical imaging domain, due to desirable factors, e.g. network matching capability, design simplicity, ease of excitation, high bandwidth and higher gain that made it an exceptional candidate compared to the other types. However, fabricating such an antenna, locating the design in the far-field region and miniaturizing the device are considered as the main challenges to design such antennas.

### A. ANTENNA DESIGN AND ANALYSIS

The main target of this work is to contribute to the solutions to overcome the limitations of the EDRH design. The proposed high-dielectric material was presented in the previous section results in efficient miniaturization and matching problems.

Regarding the fabrication and realization, the method of 3D printing has been performed using the transparent polyethylene material to reduce the costs and to fabricate a prototype to be located in the far-field region to propagate an electromagnetic (EM) plane-wave through the human body. As can be seen in Fig. 5, the extended section introduced into the structure of the proposed antenna has the length, which has been defined by the far-field distance definition as shown in equations 5 (a) and (b).

An antenna in the free-space experiences the free-space wave impedance of 377 ohms, which is determined by (1) [27] as:

$$z_m = \sqrt{\frac{\mu_0}{\varepsilon_0 \varepsilon_r}}. \tag{1}$$

where $\varepsilon_0 = 8.854 \times 10^{-12}(\frac{F}{m})$, $\mu_0 = 4\pi \times 10^{-7}(\frac{V.s}{A.m})$ are the permittivity and permeability of free-space, and $\varepsilon_r$ is the relative permittivity of the material, respectively. If the antenna is immersed in any dielectric material, the impedance would be different because of the mismatch that aims to reduce the size and reflections.

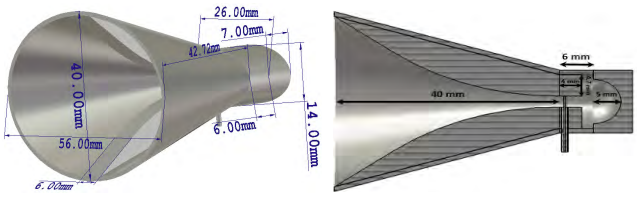


**FIGURE 4.** Modeled EDRH antenna with the aperture dimensions.

**TABLE 1.** Antenna dimensions.

| Section Name | Size (mm) | Section Name | Size (mm) |
|---|---|---|---|
| *Waveguide (Inside)* | $r_{wa0} \times r_{wb0} \times l$ 12 × 6 × 6 | *Extended Flare* | $r_{wa2} \times r_{wb2} \times l$ 42 × 32 × 40 |
| *Waveguide Ridges* | $w \times l \times h$ 6 × 4 × 4.7 | *Back (Outside)* | $r_w \times r_h \times l$ 14 × 8 × 7 |
| *Waveguide Ridges Gap* | $h$ 2.5 | *Backspace (Inside)* | $r_b$ 5 |
| *Flare (Inside)* | $r_{wa1} \times r_{wb1} \times l$ 27 × 19 × 40 | *Connector Diameters* | $r_c$ 0.4699 |
| *Flare Ridges* | $w \times l$ 6 × 42.72 | *Connector Heights* | $r_h$ 30 |

The medium's permittivity, where the antenna operates inside is also considered during the design to achieve the highest performance. This medium has a permittivity of 5.4 at 3.1 GHz. The impedance of the medium can be defined using (1) as 160.75 ohms, which reduces the size by less than half compared to free-space case [28].

The exponentially-tapered section of the antenna is important as it matches the reference impedance in the feeding point of the device, to that of the material at the aperture that is varying from 50 to 160 ohms, and was obtained by (2) [29] as follows:

$$z\,(y) = z_0 e^{ky}, (0 \le y \le L). \tag{2}$$

where $y$ is the distance from the waveguide aperture, and $L$ is the axial length of the antenna to the opening of the exponentially-tapered section, as shown in Figs. 4; $k$ is determined by (3):

$$k = \frac{1}{L} ln(\frac{Z_L}{Z_0}). \tag{3}$$

where $Z_L$ and $Z_0$ are the characteristic impedances of the double-ridged waveguide in the medium and free-space, respectively.

The dimensions of the $E$- and $H$- planes of an elliptical horn have been determined based on the dielectric material, and the equations presented in the seminal textbook [30]. The antenna is designed according to the parameters of the pyramidal horn. The antenna parameters are modified to operate in the desired frequency that set in the software shown in Table 1.

Fig. 4 presents the modeling of the developed antenna based on the measured mixture of the dielectric material data (i.e., paraffin and $TiO_2$) loaded into the software as new material by using the user dispersion option and the time-domain transient solver. The latter operates using the finite integration technique (FIT) in the CST Studio Suite software.

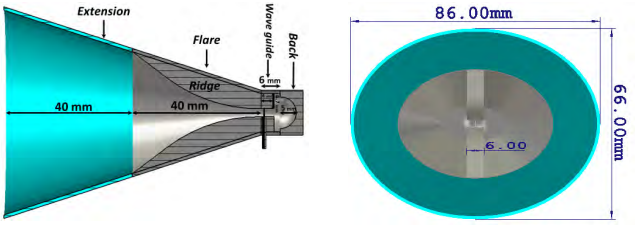


**FIGURE 5.** Modeled extended EDRH antenna with the structural labels and the dimensions for the extended section.

The next stage of the design is to propose a numerical solution for the antenna to be located in the far-field region from the targeted area of the body. This has been conducted for the in-depth penetration of the wave.

The concept can address the overlapping issue that accrues when the antenna used as a transceiver. However, the concept can be ignored in the application where the antenna is not being employed as a stand-alone transceiver. The optimal approach is to extend the outer aperture of the antenna, and to define, the antenna outer aperture length, so the scanning tissue area can be placed in the far-field region. This has added more complexity to the fabrication and realization of the device with the increased cost, but on the other hand, it has made it more stable in its operation, and free of any destructive interference signals and noise.

Equations 4 (a) and (b) define the wavelength (i.e., $\lambda$), followed by the far-field distance of the system (i.e., $d_f$) and the largest section of dimension (i.e., $D$). The wavelength is calculated as 64.5 mm. The value is obtained based on the lower frequency of 2 GHz and the measured material permittivity properties [31].

$$\lambda = \frac{c}{f\sqrt{\varepsilon_r}} = \frac{3 \times 10^8}{2 \times 10^9 \times \sqrt{5.4}} = 64.5\ mm; \quad (4a)$$

$$d_f = \frac{2 \times D^2}{\lambda} = \frac{2 \times 54^2}{64.5} = 90.4\ mm. \quad (4b)$$

The high-dielectric EDRH antenna has been extended with the pyramidal aperture length of 40 mm, based on the following equations 5 (a) and (b) that aimed to maintain the main antenna objectives (locating in a far-field region), as shown in Fig. 5. To define the outer aperture of the extended part. When the length of the extension changes, the following equations are derived:

$$r_{wa2} = 2 \times \left[\frac{r_{wa0}}{2} + \frac{r_{wa1} - r_{wa0}}{2 \times l_1} \times (l_2 + l_1)\right]; \quad (5a)$$

$$r_{wb2} = 2 \times \left[\frac{r_{wb0}}{2} + \frac{r_{wb1} - r_{wb0}}{2 \times l_1} \times (l_2 + l_1)\right]. \quad (5b)$$

where $r_{wa2}$, $r_{wb2}$, and $l$ define the width, height, and length of the horn aperture, respectively, as shown in Table 1.

The developed mixed material is selected as the background material in the simulation software to evaluate the antenna performance inside the dielectric medium based on the real data. The usual sufficient energy −6 dB point was used here to satisfy the general biomedical application [20].

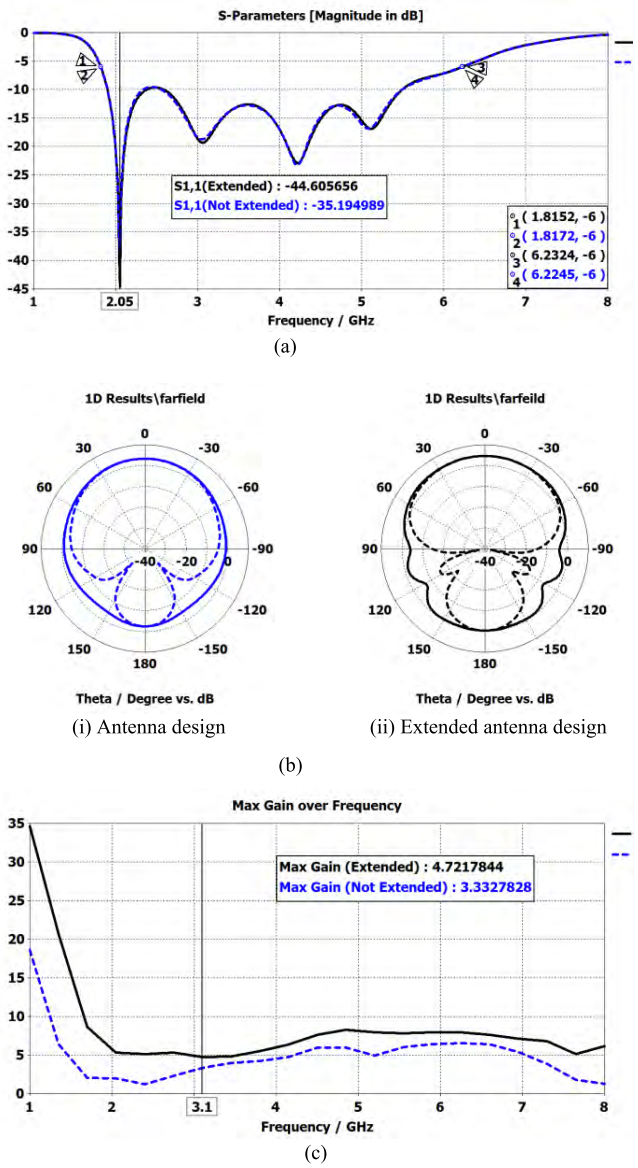


**FIGURE 6.** (a) Simulated $S_{11}$ when the antenna is inside the proposed material. (b) Magnetic (solid line) and electric (dashed line) far-field radiation patterns of the proposed antennas at the 3.1 GHz frequency with −6 and −5.2 dB sidelobe levels (SLLs). (c) Gain over the frequency range of 1–8 GHz for the antennas.

In addition, the higher energy (i.e. −10 dB) was reserved to address the worst-case scenarios. The figures of merit for the evaluation, including the reflection coefficients based on scattering ($S$)-parameters, gain, and radiation patterns have been obtained for the EDRH antennas with and without extension, as in Fig. 6.

The proposed antenna without the extension, as shown in Fig. 4, has been exhibiting the output characteristics as follows. The reflection coefficients ($S_{11}$) plots, as in Fig. 6 (a), represents a wide operating bandwidth of 4.4 GHz from 1.82 to 6.22 GHz, taking –6 dB as a reference. Moreover, the large resonant at a low frequency of 2.06 GHz that provide better penetration depth. In addition, Fig. 6 b (i) shows the radiation patterns, in the magnetic and electric fields

directions (0° and 90°Phi) at the antenna front-end. Fig. 6 (c) also depicts the gain of the antenna over the desired operating frequency range (i.e., 1 to 8 GHz).

This further depicts the minimum gain of 1.2 dB at 2.4 GHz and the maximum gain of 6.5 dB at 6.25 GHz. The mixture has been chosen as the background material for the modeled extended EDRH antenna as shown in Fig. 5. The *S*-parameter plots in Fig. 6 (a) determines a slight increase in the bandwidth, to 4.41 GHz at –6 dB, as well as a slight increase of the SLL at 3.1 GHz in the directions of 0° and 90°Phi, as in Fig. 6 b (ii). Fig. 6 (c) shows an increase in the gain with a minimum gain of 4.72 dB at 3.1 GHz, and a maximum gain of 8.26 dB at 4.85 GHz, compared with the case without extension. The extension is used to focus the beam, and to introduce a delay between the transmitted and reflected signals, in order to avoid overlapping. The extension is also found to improve the gain and directivity when compared with the design with no extension.

### B. ANTENNA EVALUATION USING THE MODELED TISSUE

In this stage of system evaluation, the arm tissue model that consists of two layers including 2 mm skin and infinite muscle has been developed, assuming there is no fat existing in this specific area having knowledge of the area has minimum volume of fat [32]. The fat layer can be ignored here to calibrate the system and to minimize the error, as it differs from one person to another in some locations; e.g., abdomen and thighs. The bone layer was not incorporated here, as the system was designed to operate at the center frequency where the pulse will be absorbed within the muscle layer.

Fig. 7 (a) depicts the proposed antenna filled with the mixture material placed on the modeled forearm tissue. The measured properties of the mixture in the desired frequency region have been loaded into the software using the new material dispersion, as shown in Fig. 7 (b).

The reflection coefficient results are also obtained for a frequency range up to 8 GHz, assumed as a calibration point, as in Fig. 7 (c). The results depict a frequency shift of 140 MHz in the intended spectrum, compared with the case where the modeled tissue is not present as shown in Fig. 6 (a), but still obtaining the same bandwidth of 4.1 GHz.

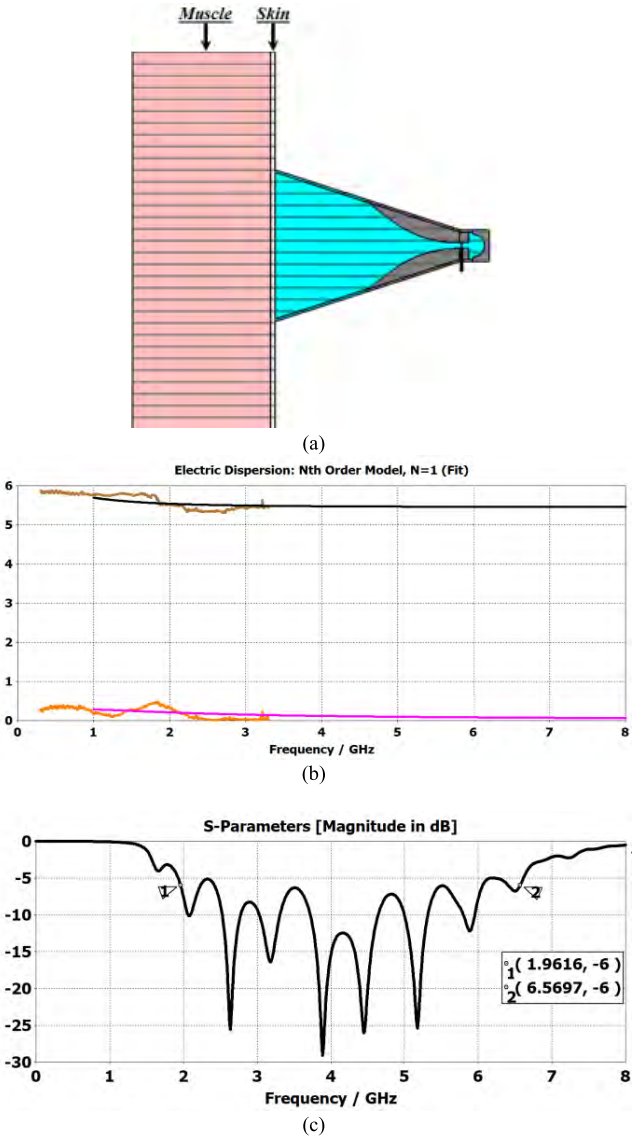


**FIGURE 7.** (a) Proposed EDRH antenna placed on the modeled forearm tissue. (b) Measured properties of the mixture loaded into the CST software. (c) Simulated $S_{11}$ of the antenna, when the fat layer does not exist.

## IV. ANTENNA FABRICATION AND MEASUREMENT

### A. ANTENNA FABRICATION AND REALIZATION

Fabrication of complex 3D-printed EDRH antenna requires an in-house 3D printer and some modification to the design, e.g. cutting the antenna symmetrically to two parts prior to printing and attaching them back together shown in Fig. 8 (a).

The Stratasys Objet30 Prime 3D printer has been used to print the prototype with a resolution of 100 $\mu$m. The prototype has been realized with a clear finish and the support material was removed by rinsing the prototype using pressurized water.

The cost of a Vero clear transparent polyethylene is $\sim$ 650 USD per kg [33]. The cost of the Vero including the support material used to 3D print the prototype is less than 50 USD.

Hence, the Objet30 printer offers cost-effective solutions for 3D printing small complex antenna structures with a high resolution. In addition, the printed EDRH antenna is painted with silver conductive paint with acceptable conductivity up to the extended part of the design shown in Fig. 8 (b). A 3 grams bottle of silver was used to metalize the prototype at a cost of fewer than 15 USD [34].

The antenna was connected to a 50-ohm cable SMA connector with an outer dimension of 1.19 mm fed and glued to the lower- and upper-ridges of the antenna, shown in Fig. 8 (b).

The two sections of the antenna were then glued together; the glued area was painted and finally filled with the

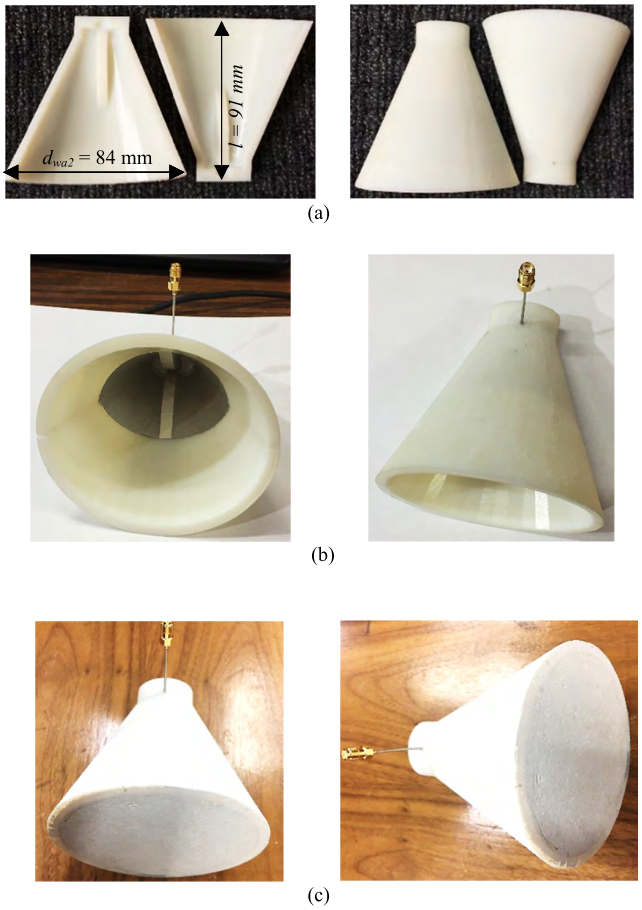


**FIGURE 8.** (a) 3D-printed EDRH antenna using the polyethylene material. (b) 3D-printed EDRH antenna, as conductive-painted and fed with a semi-ridged SMA connector. (c) 3D-printed EDRH antenna filled with the high-dielectric mixture.

high-dielectric mixture. During this process, it is placed upside down to remove any remaining bubble gaps produced during the mixing and filling process, as illustrated in Fig. 8 (c).

### B. ANTENNA MEASUREMENTS ON THE HUMAN BODY

The forearm of the body is selected as the equivalent tissue to the modeled tissue in the simulations, with regards to the nonexistence of the fat layer. The flexible coaxial cable is utilized to connect the antenna to the VNA and was calibrated to remove the cable effects using the Ecal calibration kits. The fabricated antenna filled with the mixture has been placed on the forearm location of the human's arm and the reflection coefficient results have been obtained and shown in Figs. 9 (a) and (b). The results are compared with the simulations at the first resonance, chosen to be the operating point for the antenna for better penetration to the human body for use in the biomedical applications, as shown in Fig. 9 (b). The simulation and experiment comparison results show a frequency shift of 0.4 GHz to the higher band and an increase of −3.39 dB in the magnitude at the first large resonance. This was expected due to the different effects and errors,

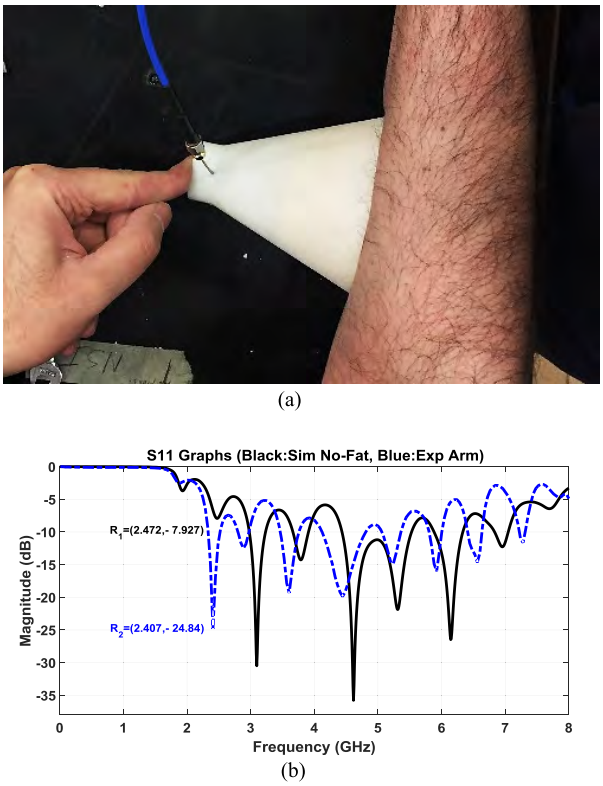


**FIGURE 9.** (a) The 3D-printed antenna placed on the arm for the calibration. (b) Black plot depicts the simulations; i.e., no fat case; and the blue dashed plot shows the measured results obtained based on the arm's case.

e.g., the fabrication process, experimental environment, and human errors could build up to the real data compared to the simulated data. It should be noted that the air gap between the antenna and body can be eliminated using the semi-solid mixture (oil and $TiO_2$) that have more or less the same dielectric constant. This removes the effect of the air gap in the real experiment. This novel method of implementing a material-filled antenna could be used in other biomedical applications that aim to scan inside the body, e.g. in abdominal fat measurement [35].

## V. DISCUSSION

This investigation has thoroughly presented the EM design and performance evaluations of a compact WB 3D-printed EDRH antenna that is filled with a novel low-conductive and high-dielectric paraffin ceramic mixture with the flexibility in shaping its form. The chosen dielectric materials mixture of paraffin and r-$TiO_2$ was heated using a lab glass and normal hot plate equipment in the lab. In addition, the materials mixed by a metallic teaspoon and poured into the antenna. This process can be performed in the cavity to avoid the bubbles created during the process, which reduces the conductivity and increase the permittivity to some extent. The in-house 3D printer with high resolution was employed to reduce the cost of such a complex antenna. Concerning, the measurements on different individual and different influences that

may introduce into the system, as the scanning area (the arm) has the layers structure (skin, fat, and muscle) that has no much different from one to another in terms of permittivity and thickness. This should not have a sufficient impact on the results; however, this can be upgraded by employing an extra calibration method (e.g. using an open-ended probe to measure the effective permittivity of the skin and using software to calibrate the results).

## VI. CONCLUSION

The miniaturized dielectric filled EDRH antenna design can be employed in any system that aims to scan and analyze a specific part of the human body. The novel high dielectric paraffin based ceramic has been conducted within the design to effectively reduce the size of the structure and to realize a high-performance, miniaturized, and low-cost device, as well as to reduce the unwanted reflections. This design incorporates the extension for locating the antenna in the far-field region of the scanning area, for the plane-waves to penetrate more directly into the body. Moreover, the antenna can operate at the lower frequency band of WB to exhibit a better penetration depth and impedance matching using the mixture for the biomedical application, which monitoring very deep inside the body is the main objective of the system.

## REFERENCES

[1] M. Ghavami, L. B. Michael, and R. Kohno, *Ultra Wideband Signals and Systems in Communication Engineering*, 2nd ed. Hoboken, NJ, USA: Wiley, Jan. 2007.

[2] R. Aiello and A. Batra, *Ultra Wideband Systems: Technologies and Applications*, 1st ed. Newnes, 2006.

[3] S. Sarjoghian, Y. Alfadhl, and X. Chen, "On the limitation of ultra-wideband technique for medical scanning systems," in *Proc. Loughborough Antennas Propag. Conf. (LAPC)*, Nov. 2016, pp. 1–4.

[4] G. Melia, *Electromagnetic Absorption by the Human Body From 1–15 GHz*. York, U.K.: Univ. York, 2013.

[5] A. W. Preece, I. Craddock, M. Shere, L. Jones, and H. L. Winton, "MARIA M4: Clinical evaluation of a prototype ultrawideband radar scanner for breast cancer detection.," *J. Med. Imag.*, vol. 3, no. 3, Jul. 2016, Art. no. 033502.

[6] M. Persson, A. Fhager, H. D. Trefná, Y. Yu, T. McKelvey, G. Pegenius, J.-E. Karlsson, and M. Elam, "Microwave-based stroke diagnosis making global prehospital thrombolytic treatment possible," *IEEE Trans. Biomed. Eng.*, vol. 61, no. 11, pp. 2806–2817, Nov. 2014.

[7] R. J. Adams and K. S. Kelleher, "Pattern calculations for antennas of elliptical aperture," *Proc. IRE*, vol. 38, no. 9, p. 1052, Sep. 1950.

[8] S. B. Cohn, "Properties of ridge wave guide," *Proc. IRE*, vol. 35, no. 8, pp. 783–788, Aug. 1947.

[9] S. C. J. Worm, "Corrugated elliptical horn antennas for the generation of radiation patterns with elliptical cross-section," Eindhoven Univ. Technol., Eindhoven, The Netherlands, Tech. Rep., May 1985.

[10] X. Zhang, "Design of conical corrugated feed horns for wide-band high-frequency applications," *IEEE Trans. Microw. Theory Tech.*, vol. 41, no. 8, pp. 1263–1274, Aug. 1993.

[11] J. C. S. Chieh, B. Dick, S. Loui, and J. D. Rockway, "Development of a Ku-band corrugated conical horn using 3-D print technology," *IEEE Antennas Wireless Propag. Lett.*, vol. 13, pp. 201–204, 2014.

[12] A. T. Mobashsher and A. Abbosh, "Three-dimensional folded antenna with ultra-wideband performance, directional radiation and compact size," *IET Microw. Antennas Propag.*, vol. 8, no. 3, pp. 171–179, Feb. 2014.

[13] B. Zhang, Y.-X. Guo, H. Sun, and Y. Wu, "Metallic, 3D-printed, K-band-stepped, double-ridged square horn antennas," *Appl. Sci.*, vol. 8, no. 1, p. 33, Jan. 2018.

[14] S. Rashid, L. Jofre, A. Garrido, G. Gonzalez, Y. Ding, A. Aguasca, J. O'Callaghan, and J. Romeu, "3-D printed UWB microwave bodyscope for biomedical measurements," *IEEE Antennas Wireless Propaga. Lett.*, vol. 18, no. 4, pp. 626–630, Apr. 2019.

[15] C. R. Garcia, R. C. Rumpf, H. H. Tsang, and J. H. Barton, "Effects of extreme surface roughness on 3D printed horn antenna," *Electron. Lett.*, vol. 49, no. 12, pp. 734–736, 2013.

[16] B. Majumdar, D. Baer, S. Chakraborty, K. P. Esselle, and M. Heimlich, "Additive manufacturing of a dual-ridged horn antenna," *Prog. Electromagn. Res. Lett.*, vol. 59, pp. 109–114, Apr. 2016.

[17] U. Schwarz, R. Stephan, and M. A. Hei, "Miniature double-ridged horn antennas composed of solid high-permittivity sintered ceramics for biomedical ultra-wideband radar applications," in *Proc. IEEE Antennas Propag. Soc. Int. Symp.*, Jul. 2010, pp. 1–4.

[18] D. Gibbins, M. Klemm, I. J. Craddock, J. A. Leendertz, A. Preece, and R. Benjamin, "A comparison of a wide-slot and a stacked patch antenna for the purpose of breast cancer detection," *IEEE Trans. Antennas Propag.*, vol. 58, no. 3, pp. 665–674, Mar. 2010.

[19] S. I. Latif, D. Flores-Tapia, S. Pistorius, and L. Shafai, "Design and performance analysis of the miniaturised water-filled double-ridged horn antenna for active microwave imaging applications," *IET Microw. Antennas Propag.*, vol. 9, no. 11, pp. 1173–1178, Aug. 2015.

[20] S. I. Latif, D. F. Tapia, D. R. Herrera, M. S. Nepote, S. Pistorius, and L. Shafai, "A directional antenna in a matching liquid for microwave radar imaging," *Int. J. Antennas Propag.*, vol. 2015, Oct. 2015, Art. no. 751739.

[21] A. L. Gioia, M. O'Halloran, A. Elahi, and E. Porter, "Investigation of histology radius for dielectric characterisation of heterogeneous materials," *IEEE Trans. Dielectr. Electr. Insul.*, vol. 25, no. 3, pp. 1064–1079, Jun. 2018.

[22] *Suppliesforcandles.Co.Uk*. Accessed: May 08, 2019. [Online]. Available: https://www.suppliesforcandles.co.uk/product/paraffin-container-wax

[23] G. F. Dionne, J. F. Fitzgerald, and R. C. Aucoin, "Dielectric constants of paraffin-wax–$TiO_2$ mixtures," *J. Appl. Phys.*, vol. 47, no. 4, pp. 1708–1709, 1976.

[24] S.-D. Mo and W. Y. Ching, "Electronic and optical properties of three phases of titanium dioxide: Rutile, anatase, and brookite," *Phys. Rev. B, Condens. Matter*, vol. 51, May 1995, Art. no. 13023.

[25] A. Wypych, I. Bobowska, M. Tracz, A. Opasinska, S. Kadlubowski, A. Krzywania-Kaliszewska, J. Grobelny, and P. Wojciechowski, "Dielectric properties and characterisation of titanium dioxide obtained by different chemistry methods," *J. Nanomater*, vol. 2014, Mar. 2014, Art. no. 124814.

[26] C. Yu, Y. Zeng, B. Yang, R. Donnan, J. Huang, Z. Xiong, A. Mahajan, B. Shi, H. Ye, R. Binions, N. V. Tarakina, M. J. Reece, and H. Yan, "Titanium dioxide engineered for near-dispersionless high Terahertz permittivity and ultra-low-loss," *Sci. Rep.*, vol. 7, p. 6639, Jul. 2017.

[27] S. Latif, S. Pistorius, and L. Shafai, "A double-ridged horn antenna design in canola oil for medical imaging," in *Proc. 2nd Int. Conf. Adv. Elect. Eng. (ICAEE)*, Dec. 2013, pp. 421–424.

[28] S. Sarjoghian, Y. Alfadhl, and X. Chen, "Compact ultra-wideband double-ridged horn antennas for medical imaging," in *Proc. Loughborough Antennas Propag. Conf. (LAPC)*, Nov. 2016, pp. 1–4.

[29] A. R. R. Mallahzadeh, A. A. Dastranj, and H. R. Hassani, "A novel dual-polarized double-ridged horn antenna for wideband applications," *Prog. Electromagn. Res. B*, vol. 1, pp. 67–80, 2008.

[30] C. A. Balanis, *Antenna Theory: Analysis and Design*, 4th ed. Hoboken, NJ, USA: Wiley, 2016.

[31] R. C. Johnson, H. A. Ecker, and J. S. Hollis, "Determination of far-field antenna patterns from near-field measurements," *Proc. IEEE*, vol. 61, no. 12, pp. 1668–1694, Dec. 1973.

[32] P. Störchle, W. Müller, M. Sengeis, S. Lackner, S. Holasek, and A. Fürhapter-Rieger, "Measurement of mean subcutaneous fat thickness: Eight standardised ultrasound sites compared to 216 randomly selected sites," *Sci. Rep.*, vol. 8, no. 1, Nov. 2018, Art. no. 16268.

[33] S. Alkaraki, Y. Gao, M. O. M. Torrico, S. Stremsdoerfer, E. Gayets, and C. Parini, "Performance comparison of simple and low cost metallization techniques for 3D printed antennas at 10 GHz and 30 GHz," *IEEE Access*, vol. 6, pp. 64261–64269, 2018.

[34] *Data Sheet*. Accessed: Apr. 30, 2019. [Online]. Available: https://www.electrolube.com/pdf/tds/044/SCP.pdf

[35] S. Sarjoghian, Y. Alfadhl, and X. Chen, "A novel wide-band reflection-based system for measuring abdominal fat in humans," in *Proc. URSI Int. Symp. Electromagn. Theory (EMTS)*, Aug. 2016, pp. 586–589.

**SIAMAK SARJOGHIAN** (GS'18) received the M.Sc. degree in embedded and distributed systems from London South Bank University, London, U.K., in 2010. He is currently pursuing the Ph.D. degree in electronic engineering from the Queen Mary University of London, London. His research interests include antennas; bioelectromagnetics; microwave circuits, devices, and systems; UWB; and embedded systems. He has authored or coauthored a number of papers in these areas.

**MD HASANUZZAMAN SAGOR** (M'16) received the B.Eng. degree (Hons.) in electronic engineering from the Queen Mary University of London (QMUL), and the Ph.D. degree from the University of Greenwich, in 2015. He is currently a Lecturer with QMUL. His research interests include the areas of applied electromagnetics, antennas, and wireless propagation. He has authored or coauthored a number of papers in these areas.

**YASIR ALFADHL** (M'09–SM'19) received the B.Eng. degree (Hons.) in telecommunication engineering, and the Ph.D. degree in electromagnetics and antennas in telecommunication engineering from the University of London, London, U.K., in 2000 and 2006, respectively. He is currently a Senior Lecturer with the School of Electronic Engineering and Computer Science (EECS), Queen Mary University of London (QMUL). He has authored and coauthored over 80 peer-reviewed publications. His research interests include microwave and THz antennas and devices, wireless communications, and bioelectromagnetics.

**XIAODONG CHEN** (F'15) received the B.Eng. degree in electronic physics from the University of Zhejiang, Hangzhou, China, in 1983, and the Ph.D. degree in microwave electronics from the University of Electronic Science and Technology of China, Chengdu, in 1988. He is currently a Professor of microwave engineering with the School of Electronic Engineering and Computer Science, Queen Mary University of London. He has coauthored four textbooks, over 150 journal papers, and 400 refereed conference papers. His research interests include microwave and THz antennas and devices, wireless communications, and bioelectromagnetics.